THE JOURNAL OF NAVIGATION (2020), **73**, 1106–1128.
doi:10.1017/S0373463320000193

Wi-Fi Fine Time Measurement: Data Analysis and Processing for Indoor Localisation

Yue Yu, Ruizhi Chen, Zuoya Liu, Guangyi Guo, Feng Ye and Liang Chen

(*State Key Laboratory of Information Engineering in Survey, Mapping and Remote Sensing, Wuhan University, 470002 Wuhan, China*)
(E-mail: ruizhi.chen@whu.edu.cn)

Indoor positioning systems have received increasing attention for supporting location-based services in indoor environments. Wi-Fi based indoor localisation has become attractive due to its extensive distribution and low cost properties. IEEE 802.11-2016 now includes a Wi-Fi Fine Time Measurement (FTM) protocol which can be used for Wi-Fi ranging between intelligent terminal and Wi-Fi access point. This paper introduces a framework of Wi-Fi FTM data acquisition and processing that can be used for indoor localisation. We analyse the main factors that affect the accuracy of Wi-Fi ranging and propose a calibration, filtering and modelling algorithm that can effectively reduce the ranging error caused by clock deviation, non-line-of-sight (NLOS) and multipath propagation. Experimental results show that the proposed calibration and filtering method is able to achieve metre-level ranging accuracy in case of line-of-sight by using large bandwidth. Estimation results also show that the proposed Wi-Fi ranging model provides an accurate ranging performance in NLOS and multipath contained indoor environment; the final positioning error is less than 2·2 m with a stable output frequency of 3 Hz.

KEYWORDS

1. Indoor Positioning. 2. Wi-Fi Fine Time Measurement. 3. Data Acquisition and Processing.

Submitted: 8 November 2018. Accepted: 23 March 2020. First published online: 4 May 2020.

1. INTRODUCTION. GNSS is widely used for positioning outdoors where it can provide metre-level localisation accuracy, while Wi-Fi signals are currently used for positioning indoors (Paziewski and Wielgosz, 2014). Improving the precision of indoor localisation with Wi-Fi signals and to support high accuracy indoor navigation has been a severe challenge, however, due to the complex and changeable indoor environment.

Multiple characteristics extracted from a Wi-Fi signal can be used for indoor localisation, such as received signal strength indication (RSSI) (Chintalapudi et al., 2010), channel impulse response (Zhang et al., 2012), time of arrival (TOA) (Xiong et al., 2015), angle of arrival (AOA) (Chuang et al., 2015) and channel state information (CSI) (Wu et al., 2013). Other techniques such as multi-source fusion (Zhuang et al., 2015) and fingerprint (He et al., 2017) can also be used in complex indoor scenarios. In 2016 IEEE 802.11 standardised the Fine Time Measurement (FTM) protocol which can provide metre-level localisation accuracy according to the Wi-Fi alliance (IEEE Std 802.11, 2016). Recently,

several Wi-Fi chipsets have provided hardware-level support for FTM and the smart phone Android P from Google has provided the platform-level support (Wi-Fi Certified Location, 2017). Besides the documentation for the IEEE802.11 standard, there are few details about implementation techniques and performance of round-trip time ranging systems or how to use the specified Wi-Fi chipsets (Banin et al., 2016).

Traditional Wi-Fi based indoor localisation methods usually use RSSI to calculate the distance between an intelligent terminal and Wi-Fi AP, or they use the fingerprint method (He et al., 2017). Compared with RSSI, Wi-Fi FTM, which measures the round-trip time (RTT) of the Wi-Fi signal between initiator and responder/AP promises the following advantages. First, Wi-Fi RTT can be more stable compared with RSSI and is less affected by multipath propagation in the line-of-sight (LOS) condition (Zhang et al., 2013). Second, it is easier to establish a relationship model between measured time and the ground truth distance after data processing (Sharp and Yu, 2014). Third, Wi-Fi FTM-based localisation does not require the preliminary efforts for obtaining environmental information compared with the fingerprint based methods (Bisio et al., 2014).

In a complex indoor environment, where the direct path between the transceiver is blocked and only non-line-of-sight (NLOS) transmission exists, the distance errors measured by Wi-Fi FTM cannot be easily eliminated due to its ranging mechanism (IEEE Std 802.11, 2016). To make matters worse, the measurement errors are in different statistics in different indoor scenarios, such as office, corridor or underground carpark (Chan et al., 2006). The accuracy of Wi-Fi FTM is also affected by bandwidth of the Wi-Fi signals. For instance, the ranging results are much more accurate using 80 MHz bandwidth than with 40 MHz bandwidth. With larger bandwidth, the ranging errors can be reduced by improving the resolution of the multipath detection (Al-Jazzar et al., 2007). Another important factor is the clock deviation error caused by initial deviation and random errors which are inconsistent with different initiators and responders and should be estimated and eliminated.

In order to solve the challenges mentioned above, a calibration and filtering algorithm is presented to eliminate the ranging error caused by clock deviation and a real-time Wi-Fi ranging model is proposed to decrease the effects of NLOS and multipath propagation. To this end, we collected data from multiple APs using different sampling rates to test the relationship between sampling rate and stability of the data. Finally, we estimated the ranging accuracy in a typical indoor environment using multiple APs and then evaluated the overall positioning performance of the proposed algorithm.

The rest of this paper is organised as follows: Section 2 will introduce some related work. Section 3 will give a theoretical framework about the principle of Wi-Fi FTM and propose a calibration, filtering and modelling algorithm. Section 4 presents a series of experiments to evaluate the accuracy and stability of the proposed algorithm. We will conclude this paper and point out our future work in Section 5.

2. RELATED WORK.

2.1. *Estimation of NLOS and multipath propagation.* Saito et al. (2016) evaluated the multipath effect in the line-of-site (LOS) condition, distinguishing the directional and polarisation characteristics estimated by the RiMax algorithm proposed in Hanssens et al. (2018). Mrstik et al. (2007) quantitatively analysed the effect of angle of inclination between the Wi-Fi station and Wi-Fi AP in tracking using RADAR. Another line of work

https://doi.org/10.1017/S0373463320000193 Published online by Cambridge University Press

(Chen et al., 2016) collected the channel frequency responses to achieve centimetre-level accuracy in the NLOS constrained indoor environment. ToneTrack (McCrady et al., 2000) implements a frequency combining algorithm to increase the bandwidth on the WARP hardware radio platform to track Wi-Fi based devices indoors. In this system, McCrady et al. proposed a triangular inequality and clustering-based outlier detection to filter the NLOS APs.

2.2. *Evaluation of time measurement based ranging systems.* Wi-Fi FTM protocol is based on the TOA and TOD methods (He et al., 2013; Rea et al., 2017) which can also be used to measure the time of flight (TOF). Banin et al. (2013) introduced how the TOF works in detail and designed a series of experiments for localisation estimation in a typical indoor environment. In order to reduce the negative impacts on unsynchronised time signal and multipath, they used EKF fusing TOF measurements with IMU to enhance the performance of the TOF system (Schatzberg et al., 2014). Dvorecki et al. (2019) proposed a 'Siamese' artificial neural network based on the machine learning approach, which gives an effective solution to the influence of low bandwidth and improves the ranging precision of Wi-Fi FTM. Niesen et al. (2017) proposed an improved dedicated short-range communication method by Wi-Fi FTM to perform outdoor inter-vehicle ranging. They discussed a timestamp compression method that discarded the most significant bits of each FTM frame.

3. THEORETICAL FRAMEWORK.

IEEE 802.11 (2016) now includes a Wi-Fi FTM protocol which allows an initiator to determine its distance from a local responder/AP. In order for an initiator to obtain its location, the initiator may perform this procedure with multiple surrounding responders whose locations are known. However, this procedure may be affected by several key factors such as clock deviation error, NLOS and multipath propagation. This section will illustrate the principle of Wi-Fi FTM and go on to give our solutions to eliminate the ranging errors caused by clock deviation, NLOS and multipath propagation. The framework of the proposed Wi-Fi FTM base data acquisition and processing algorithm is illustrated in Figure 1.

3.1. *Principle of Wi-Fi FTM.* Wi-Fi FTM protocol enables distance measurement between initiators and responders such as mobile phones and APs. The whole procedure is described as follows. First, the initiator sends a FTM request to the responder. The responder receives the request and returns an ACK signal to the initiator which indicates that the responder has received the FTM request. After that several FTM signals are sent from responder to the initiator to calculate the mean RTT. This process can be performed between several initiators and responders at the same time. Figure 2 shows the whole protocol. In this procedure, the parameter named 'FTMs per burst' can be changed to improve the FTM accuracy by multiple measurements. A single RTT in one FTM period is calculated by Equation (1):

$$\mathrm{RTT} = (t_{4\_n} - t_{1\_n}) - (t_{3\_n} - t_{2\_n}) \tag{1}$$

where n indicates one FTM structure exchange during the whole FTM procedure, t_{1_n} is the timestamp when the FTM structure is first sent by the responder, t_{2_n} is the timestamp when the FTM structure is received by the initiator, t_{3_n} is the timestamp when the initiator returns the FTM structure to the responder and t_{4_n} is the timestamp when the FTM structure is finally received by the responder. Generally, the protocol excludes the processing time on the initiator by subtracting it $(t_{3\_n} - t_{2\_n})$ from the total RTT $(t_{4\_n} - t_{1\_n})$, which represents

https://doi.org/10.1017/S0373463320000193 Published online by Cambridge University Press

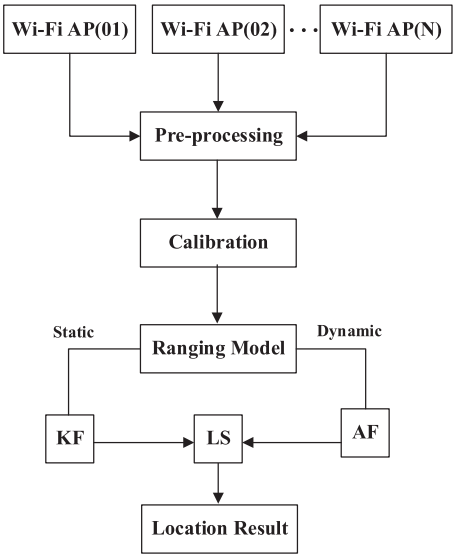

Figure 1. Framework of the proposed algorithm.

the time from the instant when the FTM structure is sent (t_{1_n}) by the responder to the instant when the FTM structure is finally received by the responder (t_{4n}). This calculation is repeated for each FTM structure exchange and the final RTT is the average over the number of FTMs per burst. In this study, the parameter of FTMs per burst was set at 30 to minimise the measurement noise so as to keep high accuracy (Ibrahim et al., 2018).

The distance between initiator and responder can be calculated by Equation (2):

$$\text{distance} = C \cdot \left[(t_{4\_n} - t_{1\_n}) - (t_{3\_n} - t_{2\_n})\right]/2 \tag{2}$$

where C indicates the speed of the radio wave.

3.2. *Analysing and processing of clock deviation error.* The clock deviation that affects the accuracy of Wi-Fi FTM generally always contains initial clock deviation and random clock error. The initial clock deviation exists before the FTM procedure and is decided by both initiator and responder, similar to TOA and DOA technology (Navarro and Najar, 2011; Shen et al., 2012). The random clock error exists during each FTM exchange and can be seen as the measurement noise. Both errors should be eliminated in order to improve the accuracy and stability of the Wi-Fi FTM.

3.2.1. *Calibration method for the initial clock deviation.* It can be observed from Figure 2 that in the first burst duration of Wi-Fi FTM, the first time the responder sends FTM information to the initiator, message FTM_1(0,0) is sent because t_{1_0} and t_{4_0} are unknown (IEEE Std 802.11, 2016). At the beginning of the following burst duration of FTM, message FTM_1(t_{1_n},t_{4_n}) is sent by the responder. However, these timestamps are not the true time instant when the signals arrive or leave the responder and initiator due to the signal processing and hardware delay. The true RTT between initiator and responder has been added with an initial time difference Δt_{delay} before the FTM procedure. Δt_{delay} in

https://doi.org/10.1017/S0373463320000193 Published online by Cambridge University Press

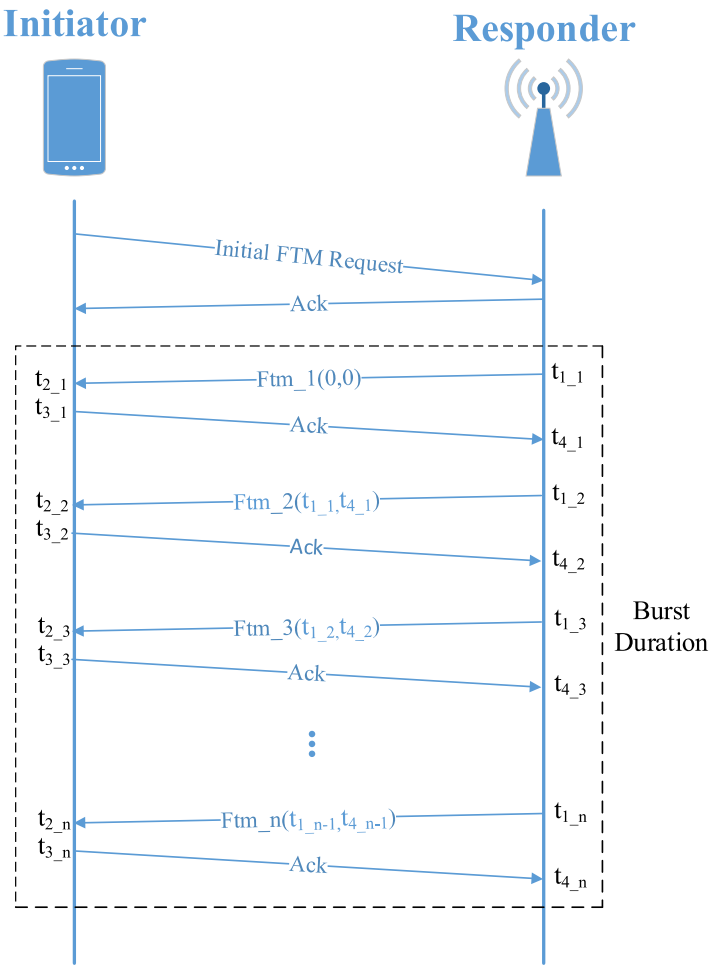

Figure 2. Duration of FTM procedure, FTMs per burst = n.

one period of RTT can be described as follows:

$$\begin{aligned} \mathrm{RTT}_{\mathrm{true}} &= (((t_{4\_n} - t_{4\_\mathrm{delay}}) - (t_{1\_n} + t_{1\_\mathrm{delay}}) - ((t_{3\_n} + t_{3\_\mathrm{delay}}) - (t_{2\_n} - t_{2\_\mathrm{delay}}))) \\ &= \mathrm{RTT}_{\mathrm{measurement}} - (t_{4\_\mathrm{delay}} + t_{1\_\mathrm{delay}}) - (t_{3\_\mathrm{delay}} + t_{2\_\mathrm{delay}}) \\ &= \mathrm{RTT}_{\mathrm{measurement}} - \Delta t_{\mathrm{delay}} \end{aligned} \tag{3}$$

In Equation (3), RTT_{true} is the true ranging result after moving $\Delta t_{\mathrm{delay}}$ from real-time measurement ranging result $\mathrm{RTT}_{\mathrm{measurement}}$, and n indicates one FTM structure exchange during the whole FTM procedure. In order to obtain RTT_{true}, calibration is needed. Since $\Delta t_{\mathrm{delay}}$ is not directly related to the ranging distance, but depends on the different hardware structure and processing methods of the signal (IEEE Std 802.11, 2016), it can be calibrated by measuring the ranging difference between measured distance and ground truth distance,

https://doi.org/10.1017/S0373463320000193 Published online by Cambridge University Press

as described in Equation (4):

$$\Delta t_{\text{delay}} = \frac{1}{\text{MC}} \sum_{i=1}^{M} (d_m(i) - d_t(i)), M = R/\Delta d \tag{4}$$

where M is the number of sampling groups, R is the effective measurement range of the responder, Δd indicates the sampling interval of distance, $d_m(i)$ is the average measure distance of each sampling group, $d_t(i)$ is the ground truth distance of each sampling, and C is the speed of radio wave. Δt_{delay} can be estimated and calibrated after large amount of data collection.

3.2.2. *Filtering of clock random error.* Random clock error exists during each FTM procedure, which causes signal fluctuation within the specific range. In general, Δt_{random} can be assumed as Gaussian-distributed variables with zero mean and variances σ^2 after calibration, which is described in Equation (5):

$$\Delta t_{\text{random}}(j) = \frac{1}{\sqrt{2\pi}\sigma} \cdot \exp\left(-\frac{j^2}{2\sigma^2}\right) \tag{5}$$

The filtering method contains two application situations. The first one is static state, which can be applied to the field of the internet of things and smart furniture. In such static situations, a Kalman filter (KF) can be applied to smooth and estimate the true value from raw data. Suppose that the measurement distance is constant, system state equation can be defined as:

$$\boldsymbol{X}(k) = \boldsymbol{A}\boldsymbol{X}(k-1) + \boldsymbol{W}(k) \tag{6}$$

where $\boldsymbol{A}$ is the state transition matrix, and $\boldsymbol{W}(k)$ is a driving noise with i dimension which contains random clock deviation.

The observation equation is defined as:

$$\boldsymbol{Z}(k) = \boldsymbol{H}\boldsymbol{X}(k) + \boldsymbol{V}(k) \tag{7}$$

where $\boldsymbol{Z}(k)$ is an observation of RTT ranging result, H is i dimensional diagonal observation matrix, and $V(k)$ is observation noise. Each matrix can be defined as:

$$\boldsymbol{Z}(k) = \begin{bmatrix} D_1 \\ D_2 \\ \dots \\ D_i \end{bmatrix}, \quad \boldsymbol{H} = \begin{bmatrix} 1 & 0 & \dots & 0 \\ 0 & 1 & \dots & 0 \\ \dots & \dots & \dots & \dots \\ 0 & 0 & \dots & 1 \end{bmatrix}, \quad \boldsymbol{V}(k) = \begin{bmatrix} E_1 \\ E_2 \\ \dots \\ E_i \end{bmatrix}$$

where i is the number of APs, and D_i is the calibrated RTT ranging results from different APs. In the LOS condition, $D_i = D_{\text{measurement}} - \Delta t_{\text{delay}} \cdot C/2$, and in the NLOS condition, D_i indicates the distance which is processed by both the calibration method and the Wi-Fi ranging model. $E_i = C \cdot \Delta t_{\text{random}}$ indicates the random ranging error.

Under these conditions, the KF is summarised as follows:

$$\text{Predict} : \boldsymbol{X}_p(k) = \boldsymbol{A}\boldsymbol{X}_e(k-1) \tag{8}$$

$$\text{Update} : \boldsymbol{X}_e(k) = \boldsymbol{X}_p(k) + \boldsymbol{K}(k) \cdot (\boldsymbol{Z}(k) - \boldsymbol{H}\boldsymbol{X}_p(k)) \tag{9}$$

$$\text{MSE} : \boldsymbol{p}_p(k) = \boldsymbol{A}\boldsymbol{p}_e(k-1)\boldsymbol{A}' + \boldsymbol{Q} \tag{10}$$

https://doi.org/10.1017/S0373463320000193 Published online by Cambridge University Press

$$\boldsymbol{P}_e(k) = \boldsymbol{P}_p(k) - \boldsymbol{K}(k)\boldsymbol{P}_p(k) \tag{11}$$

$$\text{Kalman Gain} : \boldsymbol{K}(k) = \boldsymbol{P}_p(k)\boldsymbol{H}'/(\boldsymbol{H}\boldsymbol{P}_p(k)\boldsymbol{H}' + \boldsymbol{R}) \tag{12}$$

where $P_p(k)$ is the prediction mean square error of the estimate when the current observation is not considered, $X_p(k)$ is the estimate of the RTT ranging results, $P_e(k)$ is the covariance matrix and $K(k)$ indicates the Kalman gain.

In a dynamic situation, a moving average filter is applied in the case when the initiator is moving, defined as follows:

$$y(k) = \frac{1}{N}\sum_{i=1}^{N-1} d_m(k-i) \tag{13}$$

where d_m is the real-time FTM measurement result, N is the length of the filtering window and the output $y(k)$ is the average of the measurement in the filtering window.

With the understanding of initial clock deviation and random clock error, RTT in one period can be described as follows:

$$\text{RTT}_{\text{total}} = (t_{4\_n} - t_{1\_n}) - (t_{3\_n} - t_{2\_n}) + \Delta t_{\text{delay}} + \Delta t_{\text{random}} \tag{14}$$

where $\text{RTT}_{\text{total}}$ is the final measured RTT data, and Δt_{delay} exists before ranging, which cannot be easily detected directly by hardware. Hence before we use the ranging system, some calibration measurements have to be taken to eliminate the initial clock deviation. Δt_{random} exists during the ranging process which is filtered by the KF and moving average filter proposed above.

3.3. *Model of NLOS and multipath propagation.* In a complex indoor environment, the Wi-Fi ranging results may contain NLOS distance which may not be easily estimated. The existence of NLOS errors will significantly degrade the localisation performance, hence mitigation of NLOS errors becomes an urgent task (Zhang et al., 2013; Wang et al., 2014; Xiong et al., 2015).

Wi-Fi FTM can also be affected by multipath propagation because of the low bandwidth. When the TOA-based methods are used, signal detection speed depends on the bandwidth of the Wi-Fi signal which can help to distinguish first arrival and multipath arrival (He et al., 2013a). Missing one detecting period could result in an error of several metres or more. In standard ranging systems, the proposed filtering method can help to filter out hardware/software noise, but it cannot eliminate the multipath effect that leads to estimated deviation. Especially in dynamic and complex indoor environments, moving objects could temporarily block the direct path of the transmitted signals or add more reflectors, resulting in the NLOS condition.

The output value of the single FTM responder is not sufficient to distinguish multipath propagation and NLOS errors in the procedure of real-time indoor positioning. In this paper, we consider an indoor environment with several available APs that support the Wi-Fi FTM. When a mobile phone is moving, part of the APs may be blocked in a short time, causing NLOS and multipath propagation which may not be detected because of the low bandwidth. In order to solve the problem, a Wi-Fi ranging model that contains the effects of NLOS and multipath propagation is proposed. We denote the locations of responders/APs by P_i and the location of the initiators by P, take the effect of NLOS and multipath into consideration

https://doi.org/10.1017/S0373463320000193 Published online by Cambridge University Press

and obtain the following model:

$$L_i = L_0 + \|\boldsymbol{P} - \boldsymbol{P}_i\| + n_i + d_{\text{random}} \tag{15}$$

where L_0 is the extra ranging result caused by multipath, n_i is the extra ranging distance caused by NLOS, d_{random} is the random error of measurement, calculated by Δt_{random} in Equation (5) which confront to a zero-mean Gaussian distribution with variance σ^2. We assume that $n_i$is much bigger than d_{random}, with a boundary of b_i. Moving n_i to the left side, then squaringboth sides and ignoring the d^2_{random}:

$$(L_i - n_i)^2 \approx (L_0 + \|\boldsymbol{P} - \boldsymbol{P}_i\|)^2 + 2d_{\text{random}}(L_0 + \|\boldsymbol{P} - \boldsymbol{P}_i\|) \tag{16}$$

The d_{random} can then be obtained as:

$$d_{\text{random}} \approx \frac{(L_i - n_i)^2 - (L_0 + \|\boldsymbol{P} - \boldsymbol{P}_i\|)^2}{2(L_0 + \|\boldsymbol{P} - \boldsymbol{P}_i\|)} \tag{17}$$

Then we define a function on n_i:

$$f(n_i) = \frac{|(L_i - n_i)^2 - (L_0 + \|\boldsymbol{P} - \boldsymbol{P}_i\|)^2|}{L_0 + \|\boldsymbol{P} - \boldsymbol{P}_i\|} \tag{18}$$

Least square (Gao et al., 2017) can be used to solve the above problem:

$$\min_{P,L_0} \max_{n_i} \sum_{i}^{N} \frac{f^2(n_i)}{4\sigma^2} = \min_{P,L_0} \sum_{i}^{N} \frac{[\max_{n_i} f(n_i)]^2}{4\sigma^2} \tag{19}$$

with the condition $0 < n_i < b_i$, $\max_{n_i} f(n_i)$ can be divided into two cases:

- First case: $L_i <= b_i$, then $\max_{n_i} f(n_i) = \max\{f(0), f(L_i), f(b_i)\}$;
- Second case: $L_i > b_i$, then $\max_{n_i} f(n_i) = \max\{f(0), f(b_i)\}$.

Equation (19) can then be translated as:

$$\begin{aligned} &\min_{\boldsymbol{P},L_0,\{\eta_i\}} \sum_{i=1}^{N} \eta_i \\ &s.t. \ \frac{f^2(0)}{4\sigma^2} \le \eta_i, \frac{f^2(L_i)}{4\sigma^2} \le \eta_i, \frac{f^2(b_i)}{4\sigma^2} \le \eta_i (L_i \le b_i) \end{aligned} \tag{20}$$

Introducing variables $y = \|\boldsymbol{P}\|^2$, $r = L_0^2$, $k_i = 2L_0\|\boldsymbol{P} - \boldsymbol{P}_i\|$, the following equation is obtained:

$$\begin{aligned} &\min_{\boldsymbol{P},L_0,y,r,\{\eta_i,k_i\}} \sum_{i=1}^{N} \eta_i \\ &s.t. \ \frac{(L_i^2 - y - r + 2\boldsymbol{P}_i^T\boldsymbol{P} - \|\boldsymbol{P}_i\|^2 - k_i)^2}{y + r - 2\boldsymbol{P}_i^T\boldsymbol{P} + \|\boldsymbol{P}_i\|^2 + k_i} \le 4\sigma^2\eta_i, \\ &\frac{(k_i^2 - 2L_ik_i + L_i^2 - y - r + 2\boldsymbol{P}_i^T\boldsymbol{P} - \|\boldsymbol{P}_i\|^2 - k_i)^2}{y + r - 2\boldsymbol{P}_i^T P + \|\boldsymbol{P}_i\|^2 + k_i} \le 4\sigma^2\eta_i, \end{aligned}$$

https://doi.org/10.1017/S0373463320000193 Published online by Cambridge University Press

$$\frac{(2\boldsymbol{P}_i^T\boldsymbol{P} - \|\boldsymbol{P}_i\|^2 - k_i - y - r)^2}{y + r - 2\boldsymbol{P}_i^T\boldsymbol{P} + \|\boldsymbol{P}_i\|^2 + k_i} \le 4\sigma^2\eta_i,$$
$$y = \|\boldsymbol{P}\|^2, r = L_0^2, k_i = 2L_0\|\boldsymbol{P} - \boldsymbol{P}_i\|(L_i \le b_i) \tag{21}$$

Based on the assumption that $n_i \gg |d_{\text{random}}|$, we can transform Equation (21) into a tighter problem:

$$A[P^T, y, L_0, r]^T \le f \tag{22}$$

in which

$$A = \begin{bmatrix} -2\boldsymbol{P}_1^T & 1 & 2L_1 & -1 \\ \cdots & \cdots & \cdots & \cdots \\ -2\boldsymbol{P}_N^T & 1 & 2L_N & -1 \end{bmatrix}, \quad f = \begin{bmatrix} L_1^2 - \|\boldsymbol{P}_1\|^2 \\ \cdots \\ L_N^2 - \|\boldsymbol{P}_N\|^2 \end{bmatrix}$$

Equation (22) is non-convex. With the constraints $y = \|\boldsymbol{P}\|^2, r = L_0^2$, we can apply the commonly used standard second-order cone relaxation technique to relax them as $\|\boldsymbol{P}\|^2 \le y$ and $L_0^2 \le r$. For the constraint $k_i = 2L_0\|\boldsymbol{P} - \boldsymbol{P}_i\|(L_i \le b_i)$, it is different to transform it as a convex one, so we just can get the following equation:

$$\begin{aligned} 0 \le k_i = 2L_0\|\boldsymbol{P} - \boldsymbol{P}_i\| &\le r + y - 2\boldsymbol{P}_i^T\boldsymbol{P} + \|\boldsymbol{P}_i\|^2 \\ k_i^2 = 4L_0^2\|\boldsymbol{P} - \boldsymbol{P}_i\|^2 &\le 4r(y - 2\boldsymbol{P}_i^T\boldsymbol{P} + \|\boldsymbol{P}_i\|^2) \end{aligned} \tag{23}$$

Utilising the relaxations for constraints $y = \|\boldsymbol{P}\|^2, r = L_0^2$ and the approximations in Equation (23), we can obtain a convex second-order cone program:

$$\begin{aligned} &\min_{\boldsymbol{P}, L_0, y, r, \{\eta_i, k_i\}} \sum_{i=1}^{N} \eta_i \\ &s.t. \ \frac{(L_i^2 - y - r + 2\boldsymbol{P}_i^T\boldsymbol{P} - \|\boldsymbol{P}_i\|^2 - k_i)^2}{y + r - 2\boldsymbol{P}_i^T\boldsymbol{P} + \|\boldsymbol{P}_i\|^2 + k_i} \le 4\sigma^2\eta_i, \\ &\frac{(k_i^2 - 2L_ik_i + L_i^2 - y - r + 2\boldsymbol{P}_i^T\boldsymbol{P} - \|\boldsymbol{P}_i\|^2 - k_i)^2}{y + r - 2\boldsymbol{P}_i^TP + \|\boldsymbol{P}_i\|^2 + k_i} \le 4\sigma^2\eta_i, \\ &\frac{(2\boldsymbol{P}_i^T\boldsymbol{P} - \|\boldsymbol{P}_i\|^2 - k_i - y - r)^2}{y + r - 2\boldsymbol{P}_i^T\boldsymbol{P} + \|\boldsymbol{P}_i\|^2 + k_i} \le 4\sigma^2\eta_i, \\ &\|\boldsymbol{P}\|^2 \le y, L_0^2 \le r, (23), (24) \end{aligned} \tag{24}$$

The optimal estimated values of $\|\boldsymbol{P} - \boldsymbol{P}_i\|$ and L_0 can be calculated from the above formulas and constraints.

4. EXPERIMENTS.

In this section, a real-time Wi-Fi FTM system was built up to evaluate the proposed calibration, filtering and modelling algorithm in different test scenarios. The real-time performance and accuracy of Wi-Fi FTM-based ranging and indoor localisation were then estimated to complete the evaluation of the overall algorithm framework.

https://doi.org/10.1017/S0373463320000193 Published online by Cambridge University Press

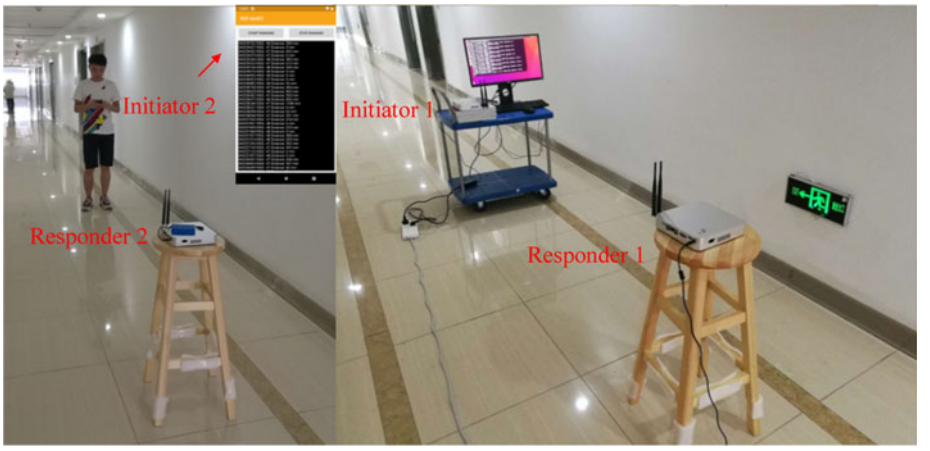

Figure 3. Wi-Fi RTT ranging system.

4.1. *Construction of Wi-Fi FTM system.* In order to analyse the performance of Wi-Fi FTM, a Wi-Fi ranging system including hardware and software support was built up, which could realise real-time data acquisition with a specified frequency. The whole ranging system is composed as follows:

4.1.1. *FTM responder/AP.* Implementation of RTT data acquisition requires hardware and software support. We chose the Intel Dual Band Wireless-AC 8260 card as the first type of AP/responder and used the Ubuntu 16.04 LTS system and Linux kernel version 4.4.0-21 as the software platform. The original driver pack does not contain the FTM response function so we needed to modify the driver and add the FTM response function. By downloading the hostapd-2.3 and opening the Wi-Fi hotspot, one RTT responder can be made. Then we chose the mobile phone VIVO NEX and VIVO X21, based on Android 8.1, which support the IEEE.802.11 FTM as the second and third type of AP. Just by opening the hotspot mode of the phone, RTT information can be obtained by the initiator.

4.1.2. *FTM initiator.* We used the same hardware and software platform as the first kind of AP responder to make a RTT initiator. By modifying the RTT ranging command and adding the FTM function into the driver, RTT information can be obtained from multiple APs by sending the ranging requests from the initiator containing MAC address, bandwidth and frequency. Only APs that support FTM can return the RTT information. Knowing the position of three or more APs and RTT information between the initiator and APs, the real-time position of the mobile initiator can be obtained. In addition, Android P provides a platform and API that can be used for RTT ranging, so we also used the Google Pixel 1 mobile phone, which has the latest Android P system installed, as another initiator. The RTT ranging system is shown in Figure 3.

In this system, several initiators are supported to use at the same time and acquire RTT data from multiple APs. Different sampling rates of RTT can be set by modifying the parameters of the ranging function.

4.2. *Calibration and filtering of clock deviation.* As discussed in Section 3, the initial clock deviation exists before the FTM procedure which causes the initial ranging error. In order to analyse the relationship between initial clock deviation and types of responders and initiators, we chose a corridor 50 m in length as the experimental scene. The responder

https://doi.org/10.1017/S0373463320000193 Published online by Cambridge University Press

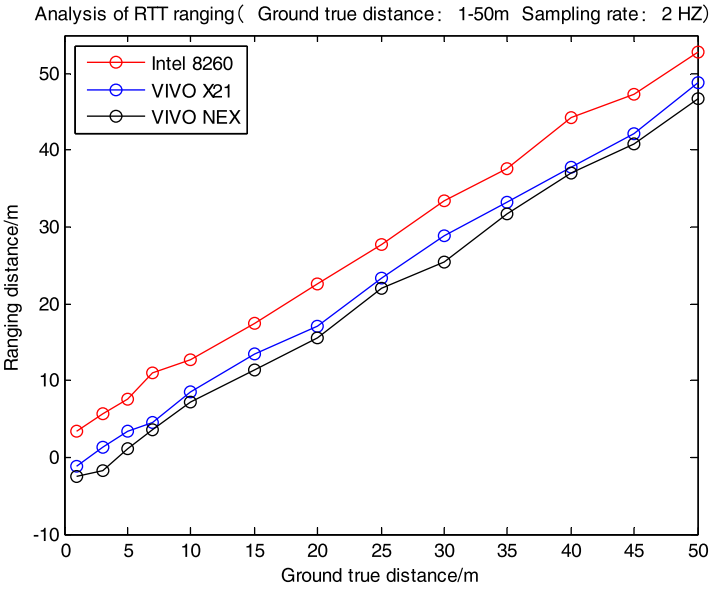

Figure 4. One initiator with three different APs.

and initiator were placed on brackets at the same height (0·8 m). The ground truth distance was marked in advance and then 2 m was set as the measuring interval when the distance is shorter than 10 m, and 5 m as the measuring interval when distance is longer than 10 m. The sampling rate was set at 2 Hz, measured for 10 min at each estimation point. RTT data was collected from three different AP responders (Intel 8260, VIVO X21, VIVO NEX) with the same initiator (Intel 8260). The average result at each estimation point is shown in Figure 4. Two different kinds of initiators (Intel 8260 and Pixel 1) were then used to collect RTT data from the same AP (Intel 8260), and the average result at each estimation point is shown in Figure 5.

It can be found by comparing Figures 4 and 5 that the initial clock deviation is influenced by both initiator and responder, thus calibration is needed before ranging. In order to calibrate the initial clock deviation, a playground was chosen as the calibration scene, as shown in Figure 6, where the multipath effect was minimised. The length of 50 m was set as the effective measurement range, different calibration intervals were set as mentioned above, with sampling rate at 2 Hz. RTT data was collected from an AP responder with 2·4 GHz frequency and 20 MHz bandwidth. Each group of data was collected for 10 min. The ranging bias of each group can be calculated by subtracting the true distance from the average ranging distance. After removing the maximum and minimum deviation of bias, we chose the average bias of the remaining data as the initial clock deviation of RTT. take into the raw data of ranging bias, the results are shown in Figure 7.

It can be seen in Figure 7 that the initial clock deviation has been effectively corrected after calibration. It can also be observed that, with longer ranging distance, the accuracy of the RTT signal does not decline in the LOS condition due to its measuring mechanics. However, several factors such as bandwidth, frequency and hardware condition can affect the initial clock deviation of Wi-Fi FTM. Therefore, when changing parameters of the AP responder or initiator, the same calibration procedure should be followed. We compared

https://doi.org/10.1017/S0373463320000193 Published online by Cambridge University Press

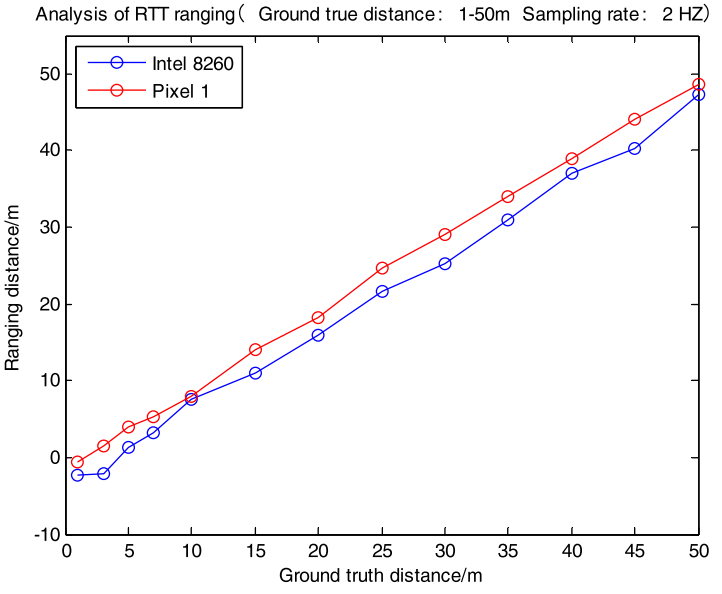

Figure 5. One AP with two different initiators.

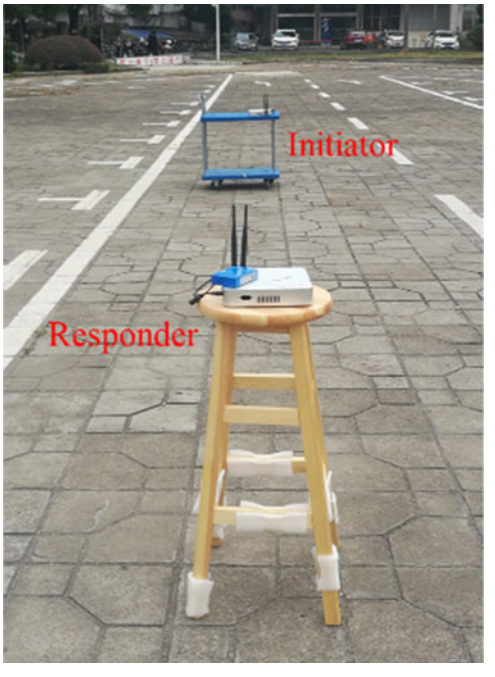

Figure 6. Calibration field.

several APs with different chipsets, bandwidths and frequencies, as shown in Table 1. We then evaluated the accuracy and stability of the calibrated data collected from Wi-Fi card A and Wi-Fi card B, and another Wi-Fi card A was used as the initiator. We used the same

https://doi.org/10.1017/S0373463320000193 Published online by Cambridge University Press

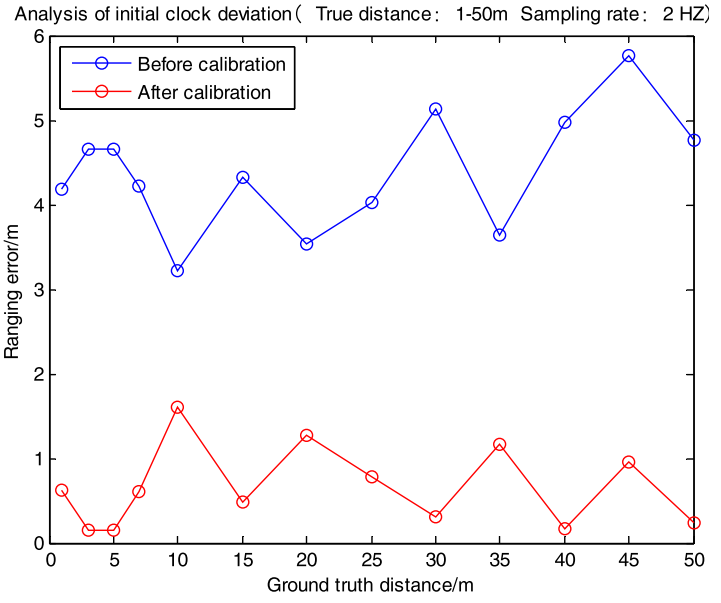

Figure 7. Comparison of errors before and after calibration.

Table 1. Influence of different factors on initial clock deviation.

AP category	20 MHz(2·4 G)	40 MHz(2·4 G)	40 MHz(5 G)	80 MHz(5 G)
Wi-Fi card A	−6 · 21 m	−4 · 56 m	Not supported	Not supported
Wi-Fi card B	Not supported	Not supported	−1 · 74 m	−1 · 07 m
Mobile phone 1	−1 · 86 m	Not supported	Not supported	Not supported
Mobile phone 2	−1 · 35 m	Not supported	Not supported	Not supported

calibration interval as in Figure 7 and obtained the calibrated ranging results shown in Figure 8. It can be seen in Figure 8 that the results of Wi-Fi FTM show greater accuracy and stability when using frequency of 5 GHz and bandwidth of 80 MHz. Metre-level ranging accuracy can be achieved with these settings.

We then designed experiments for the elimination of random error in two situations. The first is stationary state, where we set 2 m as the ground truth distance, using KF defined in Section 3. The results are shown in Figure 9. We then processed the dynamic RTT data by using the moving average filter in Equation (13), with a window size of 10. A corridor 50 m in length was chosen as the experimental scene. We used the Google Pixel 1 phone as the initiator and an Intel 8260 wireless card as AP. After calibrating the initial clock deviation, going back and forth along the corridor, and keeping the phone at the same height as the AP, the RTT ranging result is shown in Figure 10.

It can be observed in Figures 9 and 10 that random clock error can be effectively reduced using KF and moving average filter in different conditions.

https://doi.org/10.1017/S0373463320000193 Published online by Cambridge University Press

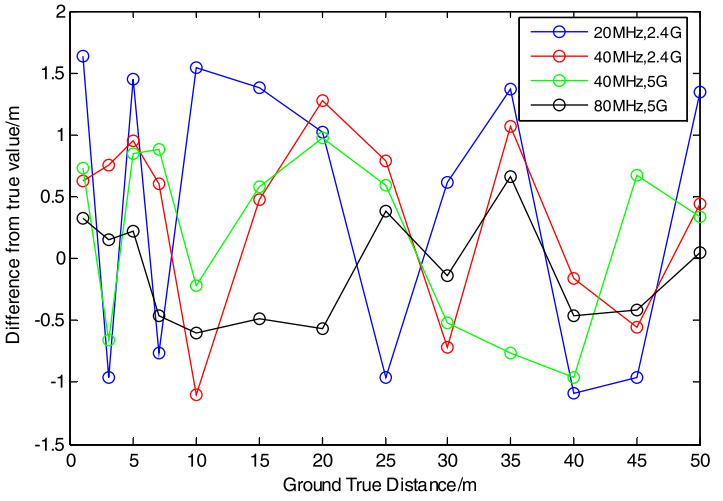

Figure 8. Comparison of ranging errors.

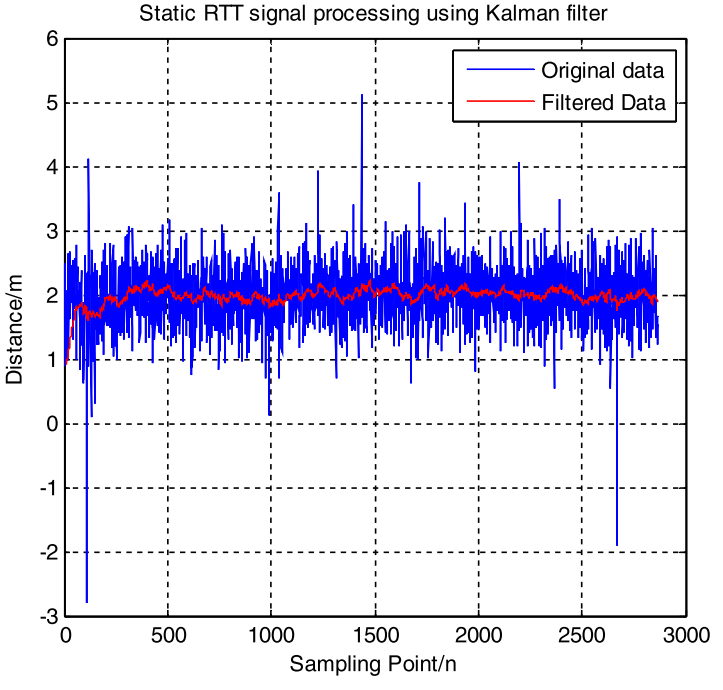

Figure 9. The performance of KF in static condition.

4.3. *Evaluation of multipath and NLOS models.*

4.3.1. *Effect of multipath in case of LOS.* We choose four typical indoor scenarios: meeting room, corridor, underground carpark and mall hall (see Figure 11), to estimate the relationship between ranging accuracy and multipath in the LOS condition, with the same AP and Google Pixel 1 as the initiator. The evaluation distance was set at 20 m, and the

https://doi.org/10.1017/S0373463320000193 Published online by Cambridge University Press

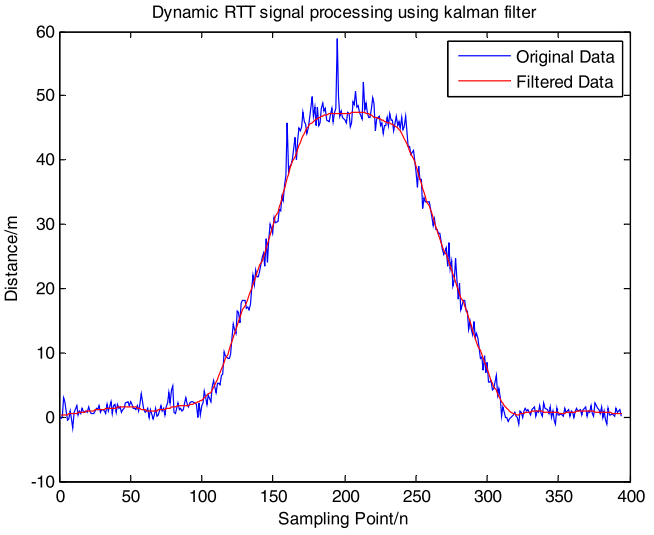

Figure 10. Dynamic RTT signal processing using moving average filter.

sampling intervals as 1 m, 3 m, 5 m, 7 m, 10 m, 12 m, 14 m, 16 m, 18 m and 20 m, as shown in Figure 12. Data was collected with a sampling rate of 5 Hz for 2 min for each group. After filtering out the extreme values and calculating the average error of each group, the results were as shown in Figure 12. It can be observed in Figure 12 that, under the condition of LOS, ranging error was generally similar among different indoor scenarios and was further reduced by the proposed Wi-Fi ranging model.

4.3.2. *Analysis of NLOS error.* NLOS is usually regarded as one kind of multipath effect, and these kinds of multiple reception cannot be eliminated easily just by the moving average filter in Equation (13). In dynamic indoor environments, moving objects could temporarily block the direct path of transmitted signals or add reflected signal which can result in extra ranging errors.

We choose three situations to test the accuracy and stability of RTT data under the NLOS condition. The test environment was an outdoor carpark. The obstacle in the first situation was two of the researchers standing together, to simulate positioning in a shopping mall. In the second situation, the obstacle was a sheet of glass or non-metallic material to simulate positioning in an office. In the third a metallic sheet was used to simulate positioning in an underground carpark. The three situations are shown in Figure 13. Over a distance of 10 m, the test intervals between initiator and obstruction were set at 1 m, 2 m, 3 m, 5 m, 7 m and 9 m. The results are shown in Figure 14.

It can be observed in Figure 14 that obstacles blocking the direct propagation path of the signal can cause additional ranging error compared with the LOS condition. Metallic obstacles can affect the ranging accuracy whether they are near the AP or initiator, while the ranging error caused by human bodies (pedestrians) and non-metallic obstacles was much smaller.

4.4. *Evaluation of Wi-Fi FTM-based indoor localisation.* In this section, we evaluate the real-time performance and stability of RTT signal from tests conducted in a typical indoor environment, and then proceed to realise the Wi-Fi FTM-based indoor localisation framework proposed in this paper. The experiment was conducted in a rectangular office,

https://doi.org/10.1017/S0373463320000193 Published online by Cambridge University Press

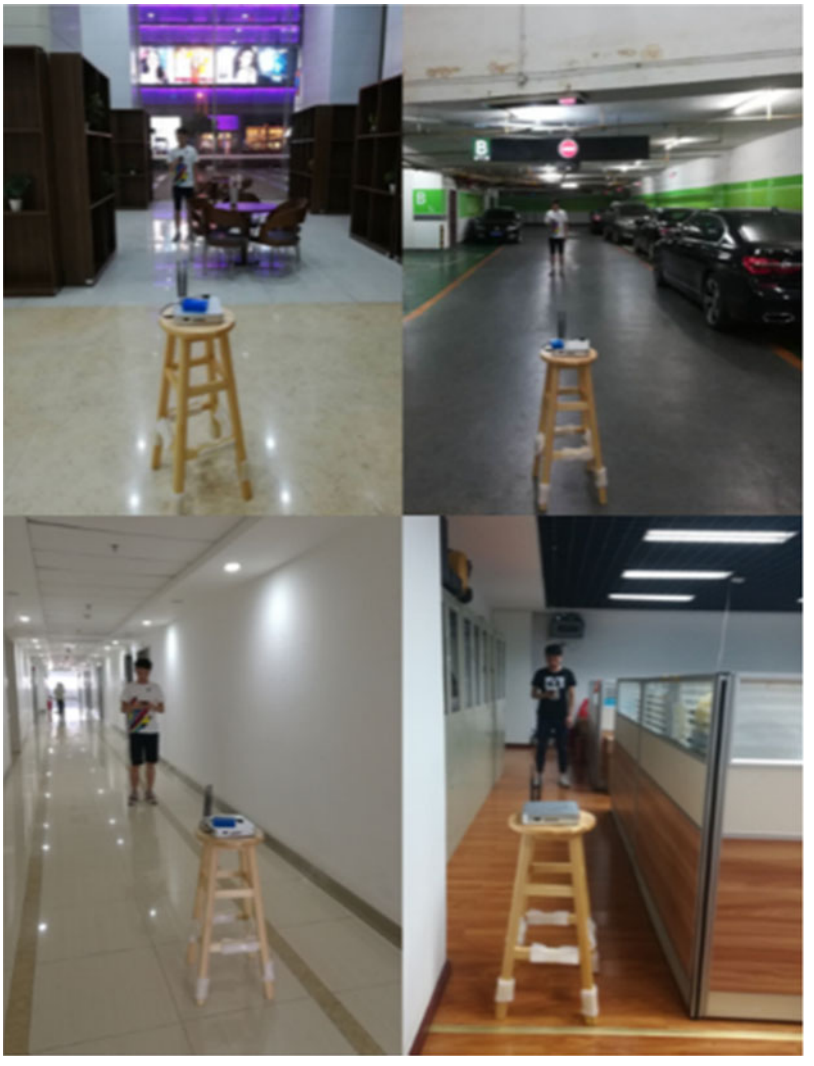

Figure 11. Four typical indoor scenarios.

in which we fixed four APs in different locations, ensuring that the RTT data could be acquired anywhere in the office (15 m ∗ 15 m). The relative location of each AP is shown in Figure 15.

4.4.1. *Analysis of real-time performance.* We used a Google Pixel 1 phone operating on the newest Android P system as the initiator, then collected RTT data from the four APs in the office using the Wi-Fi ranging API. All the APs had fixed the initial clock deviation and modified the initial clock deviation defined in Equation (5) by subtracting the corresponding initial clock deviation parameters from each AP. We then estimated the maximum real-time sampling rate of RTT data from multiple APs which can truly get in case of 2·4 GHz, 20 MHz, and estimated the stability of the data under different sampling rates. We began with a sampling rate of 0·5 Hz, then improved the sampling rate to 10 Hz,

https://doi.org/10.1017/S0373463320000193 Published online by Cambridge University Press

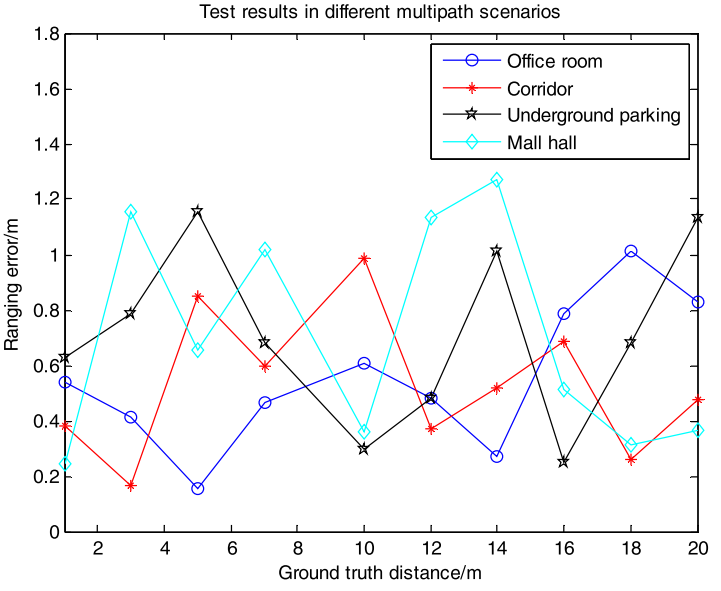

Figure 12. Comparison of ranging error.

Figure 13. NLOS situations.

choosing reference point 7 (see 4.4.2 below) as the data collection point, calculated the maximal sampling rate actually achieved after removing the abnormal measured values. The results are shown in Figure 16.

It can be observed in Figure 16 that improving the speed of sending the FTM ranging request does not positively correlate with the actual sampling rate. The success rate of sampling significantly declined when the sampling rate was improved to higher than 5 Hz and the average ranging error also increased when the sampling rate was higher than 3 Hz.

After comprehensively considering the real-time performance and stability of the measured data, we chose 3 Hz as the sampling rate used. We also found a few extreme values such as 'distance = $2 * 10^5$ m' or zero value, which can be eliminated by the threshold set in advance.

https://doi.org/10.1017/S0373463320000193 Published online by Cambridge University Press

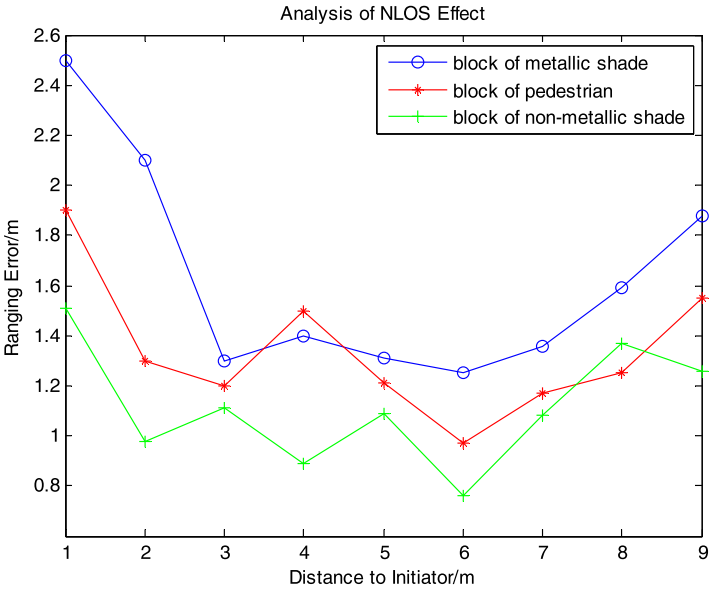

Figure 14. Ranging error caused by NLOS.

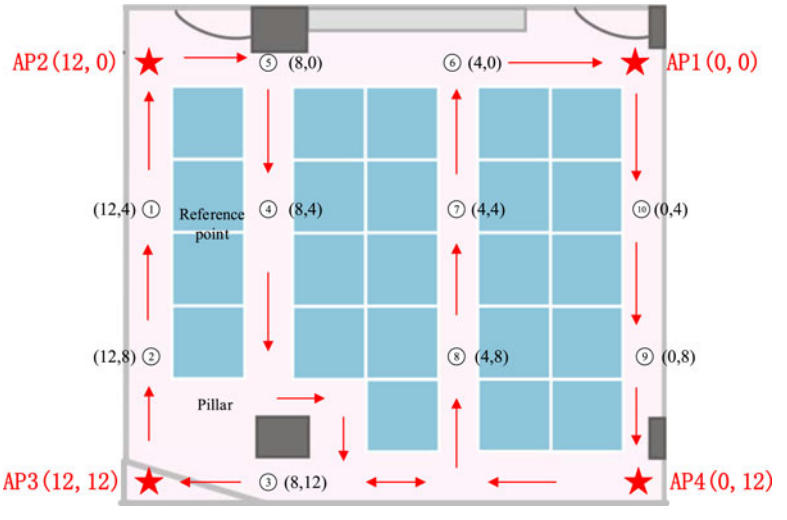

Figure 15. Locations of APs and reference points.

4.4.2. *Estimation of FTM-based indoor localisation.* We evaluated the accuracy of indoor localisation after estimating the real-time ranging performance and chose the Wi-Fi FTM sampling rate as 3 Hz. The location of the mobile phone can be calculated using real-time RTT information and the locations of the fixed APs deployed in the office. We began the experiment in a typical indoor environment (15 m ∗ 15 m) as the test scenario with typical causes of NLOS and multipath propagation, such as glass, partitions, and two

https://doi.org/10.1017/S0373463320000193 Published online by Cambridge University Press

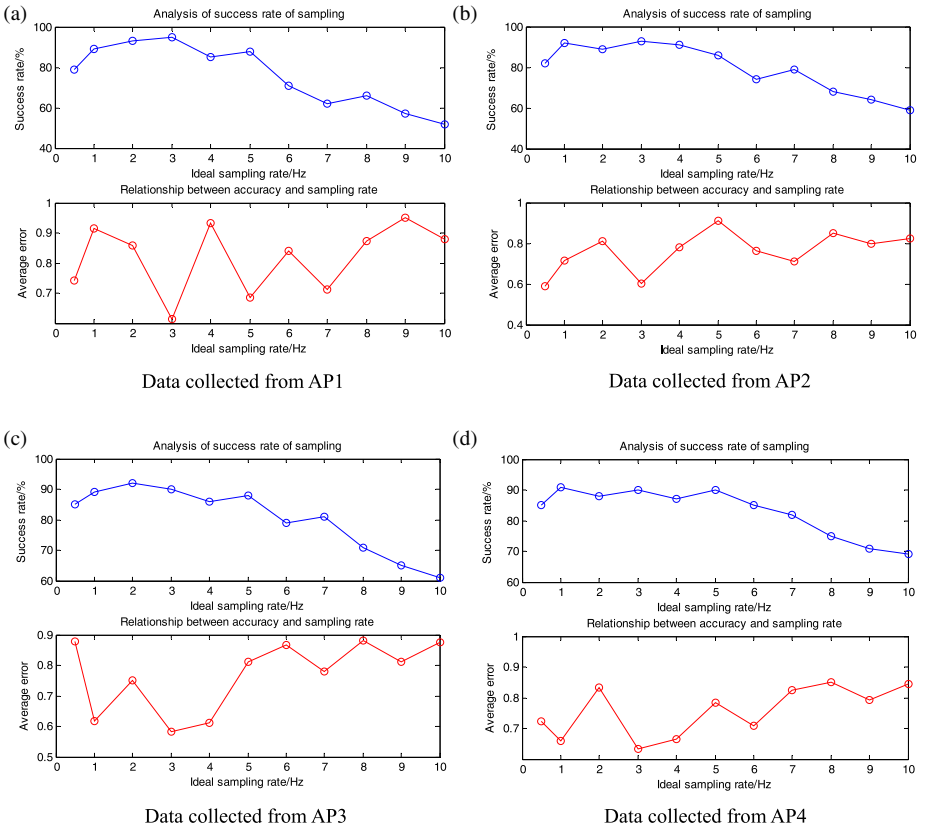

Figure 16. Analysis of continuity and stability of RTT data: (a) data collected from AP1, (b) data collected from AP2, (c) data collected from AP3, (d) data collected from AP4.

wall columns. We fixed four APs in the office and ensured that the Wi-Fi signal covered the whole area. The position of each AP is show in Figure 15.

The calibrated RTT data acquired from the deployed APs could still be affected by NLOS and multipath propagation without the ranging model. We choose 10 reference points to evaluate the accuracy of the proposed Wi-Fi ranging model. The location of each reference point is shown in Figure 15. AP3 was sometimes obscured by the pillar, causing NLOS error. The Google Pixel 1 phone was set on a 1·5 m high stand. With a sampling rate of 3 Hz, we collected data for 5 min at each reference point and calculated the average results. The raw data and processed data, which have subtracted the ground truth distance, are compared in Table 2.

It can be observed in Table 2 that the obscured AP3 caused extra ranging error at reference points 3, 8, 9 and 10 because of NLOS, while the proposed Wi-Fi ranging model can effectively improve the ranging accuracy of Wi-Fi FTM when direct transmission path is lacking. The KF can further reduce the Gaussian noise under static condition.

We then used the classical least squares trilateration algorithm (Liu et al., 2007) to calculate the real-time 2D position by Google Pixel 1 under dynamic conditions after data calibration and modelling. We set the position coordinate output frequency to 3 Hz and

https://doi.org/10.1017/S0373463320000193 Published online by Cambridge University Press

Table 2. Comparison of ranging error before and after using ranging model.

	AP1_Before	AP1_After	AP2_Before	AP2_After	AP3_Before	AP3_After	AP4_Before	AP4_After
1	0·81	0·76	0·63	0·65	0·96	0·87	1·13	1·02
2	0·58	0·62	0·72	0·75	0·83	0·71	1·28	0·96
3	2·68	1·21	2·19	1·58	0·75	0·72	0·97	0·88
4	1·12	1·09	0·74	0·71	0·82	0·69	1·07	1·11
5	0·68	0·72	0·96	0·87	1·25	1·11	0·84	0·67
6	0·88	0·76	1·18	1·03	1·85	1·24	0·81	0·77
7	1·14	0·96	0·71	0·75	1·07	0·86	0·62	0·54
8	0·86	0·72	0·91	0·92	2·68	1·39	1·31	1·02
9	0·98	0·94	1·15	0·88	2·88	1·54	0·75	0·81
10	0·76	0·68	1·09	0·96	1·93	1·07	0·61	0·63

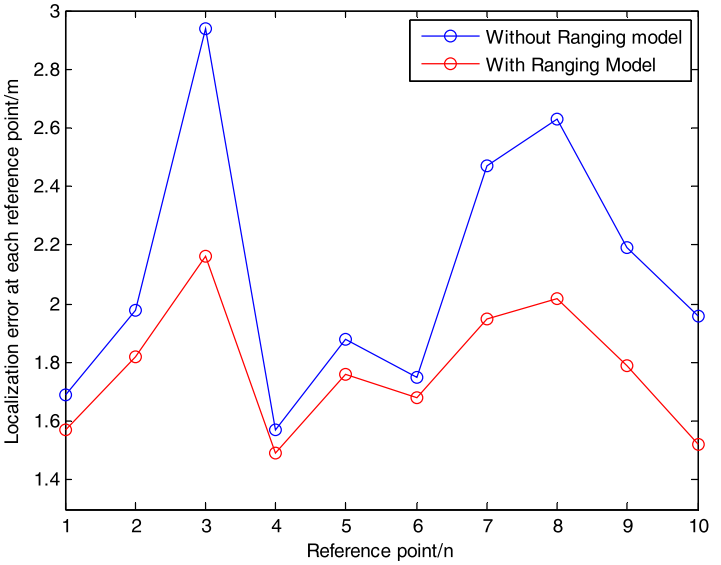

Figure 17. Localisation accuracy at each reference point.

obtained the mean positioning error result by choosing the above 10 reference points which have known 2D position, as shown in Figure 15. The tester began with the location of AP1, and passed in turn through reference points 10, 9, 3, 2, 1, 5, 4, 8, 7, 6 and then returned to the location of AP1; the reference route is shown in Figure 15. The real-time calculated localisation result was recorded when passing each reference point and the test route was repeated 10 times by different people. The average positioning error at each reference point is shown in Figure 17.

It can be observed in Figure 17 that the proposed Wi-Fi ranging model effectively improved the accuracy and stability of Wi-Fi based indoor localisation especially in case of NLOS; the average positioning error is lower than 2·2 m.

https://doi.org/10.1017/S0373463320000193 Published online by Cambridge University Press

5. CONCLUSION. The IEEE802.11 Wi-Fi FTM protocol introduced a new research direction for Wi-Fi based indoor positioning. This paper proposes a framework of Wi-Fi RTT data acquisition and processing that can be used for accurate indoor localisation. First, the Wi-Fi RTT ranging system containing responders and initiators that support the Wi-Fi FTM protocol was built up. Then the initial and random clock deviation of the RTT signal were calibrated and eliminated after data measurement and pre-processing. A real-time Wi-Fi ranging model was proposed to estimate the error caused by NLOS and multipath propagation. After that, a rectangular working office wasselected as indoor evaluation site and four APs were deployed at different locations in the office. Real-time RTT data from these APs was acquired by an Android P-based Google Pixel 1 phone and the least squares trilateration algorithm was used to obtain the real-time 2D position.

The whole framework and experiment presented in this paper shows that metre-level RTT ranging results can be obtained in the LOS condition using large bandwidth, and accurate localisation results can be achieved within 2·2 m. With the expansion of hardware functions, more and more Wi-Fi chipsets in mobile devices are expected to support large bandwidth – some can reach 160 MHz or more –, which brings an increasing accuracy of Wi-Fi ranging and Wi-Fi FTM-based indoor localisation. Subsequent to the work presented in this paper, the authors will continue with research on minimising the effect of multipath and NLOS through hardware and algorithms. The aim is to realise a universal localisation algorithm that can adapt to different indoor environments by merging multiple sources of information, such as RSSI, AOA and CSI, and achieve metre-level indoor localisation accuracy.

ACKNOWLEDGEMENTS

This work was supported by the National Key Research and Development Program of China (grant no. 2016YFB0502200 and 2016YFB0502201) and the NSFC (grant no. 91638203), Innovative Team Program funded by Hubei Province (grant no. 2018CFA007).

REFERENCES

Al-Jazzar, S., Caffery, J. and You, H. R. (2007). Scattering-model-based methods for TOA location in NLOS environments. *IEEE Transactions on Vehicular Technology*, 56(2), 583–593.

Alsindi, N. A., Alavi, B. and Pahlavan, K. (2008). Measurement and modeling of ultrawideband TOA-based ranging in indoor multipath environments. *IEEE Transactions on Vehicular Technology*, 58(3), 1046–1058.

Banin, L., Schatzberg, U. and Amizur, Y. (2013). Next Generation Indoor Positioning System Based on WiFi Time of Flight. In *Proceedings of 26th Int. Tech. Meeting Satellite Division Inst. Navigat.(ION GNSS+)*, pp. 975–982.

Banin, L., Schatzberg, U. and Amizur, Y. (2016). Wi-Fi FTM and Map Information Fusion for Accurate Positioning. In *2016 International Conference on Indoor Positioning and Indoor Navigation*, Sapporo, Japan.

Bialer, O., Raphaeli, D. and Weiss, A. J. (2011). Efficient time of arrival estimation algorithm achieving maximum likelihood performance in dense multipath. *IEEE Transactions on Signal Processing*, 60(3), 1241–1252.

Bisio, I., Cerruti, M., Lavagetto, F., Marchese, M., Pastorino, M., Randazzo, A., et al. (2014). A trainingless WiFi fingerprint positioning approach over mobile devices. *IEEE Antennas & Wireless Propagation Letters*, 13(1), 832–835.

Burgess, S., Kuang, Y. and Astrom, K. (2013). TOA sensor network calibration for receiver and transmitter spaces with difference in dimension. *Signal Processing*, 107(C), 33–42.

Chan, Y. T., Tsui, W. Y. and So, H. C. (2006). Time-of-arrival based localization under NLOS conditions. *IEEE Transactions on Vehicular Technology*, 55(1), 17–24.

Chen, C., Chen, Y. and Han, Y. (2016). Achieving centimeter-accuracy indoor localization on WiFi platforms: A multi-antenna approach. *IEEE Internet of Things Journal*, 4(1), 122–134.

Chintalapudi, K., Iyer, A. P. and Padmanabhan, V. N. (2010). Indoor Localization Without the Pain. *Sixteenth International Conference on Mobile Computing and Networking*. ACM, Chicago, USA.

Chuang, S. F., Wu, W. R. and Liu, Y. T. (2015). High-resolution AOA estimation for hybrid antenna arrays. *IEEE Transactions on Antennas & Propagation*, 63(7), 2955–2968.

Dvorecki, N., Bar-Shalom, O., Banin, L. and Amizur, Y. (2019). A Machine Learning Approach for Wi-Fi RTT Ranging. *Proceedings of the 2019 International Technical Meeting of The Institute of Navigation*, January 28–31, Hyatt Regency Reston, Reston, Virginia.

Gao, S., Zhang, F. and Wang, G. (2017). NLOS error mitigation for TOA-based source localization with unknown transmission time. *IEEE Sensors Journal*, PP(99), 1–1.

Hamilton, B. R., Ma, X., Zhao, Q. and Xu, J. (2008). ACES: Adaptive Clock Estimation and Synchronization Using Kalman Filtering. *International Conference on Mobile Computing and Networking*, MOBICOM 2008, San Francisco, California, USA.

Hanssens, B., Tanghe, E. and Gaillot, D. P., Liénard, M., Oestges, C., Plets, D., Martens, L. and Joseph, W. (2018). An extension of the RiMAX multipath estimation algorithm for ultra-wideband channel modeling. *EURASIP Journal on Wireless Communications & Networking*, 2018(1), 164.

He, J., Geng, Y., Liu, F. and Xu, C. (2014). CC-KF: Enhanced TOA performance in multipath and NLOS indoor extreme environment. *Sensors Journal IEEE*, 14(11), 3766–3774.

He, J., Pahlavan, K., Li, S. and Wang, Q. (2013). A testbed for evaluation of the effects of multipath on performance of TOA-based indoor geolocation. *IEEE Transactions on Instrumentation & Measurement*, 62(8), 2237–2247.

He, S. and Chan, S. H. G. (2015). Wi-Fi fingerprint-based indoor positioning: Recent advances and comparisons. *IEEE Communications Surveys & Tutorials*, 18(1), 466–490.

He, Z., Ma, Y. and Tafazolli, R. (2013). Improved High Resolution TOA Estimation for OFDM-WLAN Based Indoor Ranging. *IEEE Wireless Communications Letters*, 2(2), 163–166.

Ibrahim, M., Liu, H., Minitha Jawahar, V. N., et al. (2018). Verification: Accuracy Evaluation of Wi-Fi Fine Time Measurements on an Open Platform. *Proceedings of the 24th Annual International Conference on Mobile Computing and Networking*, New Delhi, India.

IEEE Std 802.11 (2016) IEEE Standard for Information Technology – Telecommunications and Information Exchange between Systems. Local and Metropolitan Area Networks – Specific Requirements – Part 11: Wireless LAN Medium Access Control (MAC) and Physical Layer (PHY) Specifications. (Revision of IEEE Std 802.11-2012). pages 1–3534, December 2016.

Li, X. and Pahlavan, K. (2004). Super-resolution TOA estimation with diversity for indoor geolocation. *IEEE Transactions on Wireless Communications*, 3(1), 224–234.

Liu, H., Darabi, H., Banerjee, P. and Liu, J. (2007). Survey of wireless indoor positioning techniques and systems. *IEEE Transactions on Systems Man & Cybernetics Part C*, 37(6), 1067–1080.

McCrady, D. D., Doyle, L. Forstrom, H., Dempsey, T. and Martorana, M. (2000). Mobile ranging using low-accuracy clocks. *IEEE Transactions on Microwave Theory and Techniques*, 48(6), 951–958.

Mrstik, A. V. and Smith, P. G. (1978). Multipath limitations on low-angle radar tracking. *IEEE Transactions on Aerospace and Electronic Systems*, 14(1), 85–102.

Navarro, M. and Najar, M. (2011). Frequency domain joint TOA and DOA estimation in IR-UWB. *IEEE Transactions on Wireless Communications*, 10(10), 1–11.

Niesen, U., Ekambaram, V. N., Jose, J. and Wu, X. (2017). Intervehicle Range Estimation from Periodic Broadcasts. 66, pp. 10637–10646.

Paziewski, J. and Wielgosz, P. (2014). Assessment of GPS + Galileo and multi-frequency Galileo single-epoch precise positioning with network corrections. *Gps Solutions*, 18(4), 571–579.

Rea, M., Fakhreddine, A. and Giustiniano, D. (2017). Filtering Noisy 802.11 Time-of-Flight Ranging Measurements from Commoditized WiFi Radios. *IEEE/ACM Transactions on Networking*, 2017, 1–14.

Saito, K., Takada, J. I. and Kim, M. (2016). Characteristics Evaluation of Dense Multipath Component in 11GHz-Band Indoor Environment. *2016 10th European Conference on Antennas and Propagation (EuCAP)*, IEEE, 2016.

Schatzberg, U., Banin, L. and Amizur, Y. (2014). Enhanced WiFi ToF indoor Positioning System with MEMS-Based INS and Pedometric Information. In *Proceedings of 2014 IEEE/ION Position, Location and Navigation Symposium-PLANS 2014*, pp. 185-192.

Schmidt, R. (1986). Multiple emitter location and signal parameter estimation. *IEEE Transactions on Antennas & Propagation*, 34(3), 276–280.

Sharp, I. and Yu, K. (2014). Indoor TOA error measurement, modeling, and analysis. *IEEE Transactions on Instrumentation & Measurement*, 63(9), 2129–2144.

Shen, J., Molisch A, F. and Salmi, J. (2012). Accurate passive location estimation using TOA measurements. *IEEE Transactions on Wireless Communications*, 11(6), 2182–2192.

Wang, G., Chen, H., Li, Y. and Ansari, N. (2014). NLOS error mitigation for TOA-based localization via convex relaxation. *IEEE Transactions on Wireless Communications*, 13(8), 4119–4131.

Wi-Fi Certified Location. (2017). https://google/BSUCdG. Accessed 9 September 2018.

Wu, K., Xiao, J., Yi, Y., Chen, D., Luo, X. and Ni, L. M. (2013). CSI-based indoor localization. *IEEE Transactions on Parallel & Distributed Systems*, 24(7), 1300–1309.

Xiong, J., Sundaresan, K. and Jamieson, K. (2015). ToneTrack: Leveraging Frequency-Agile Radios for Time-Based Indoor Wireless Localization. *MobiCom 2015. Proceedings of the 21st Annual International Conference on Mobile Computing and Networking*, Association for Computing Machinery, pp. 537–549.

Xiong, W., Liu, C., Hu, S. and Li, S. (2015). High resolution TOA estimation based on compressed sensing. *Wireless Personal Communications*, 84(4), 1–14.

Yang, Z., Zhou, Z. and Liu, Y. (2013). From RSSI to CSI: Indoor localization via channel response. *ACM Computing Surveys (CSUR)*, 46(2), 1–32.

Yi, L., Razul, S. G., Lin, Z. and Chong, M. S. (2013). Target tracking in mixed LOS/NLOS environments based on individual measurement estimation and LOS detection. *IEEE Transactions on Wireless Communications*, 13(1), 99–111.

Yin, F., Fritsche, C., Gustafsson, F. and Zoubir, A. M. (2013). TOA-based robust wireless geolocation and Cramér-Rao lower bound analysis in harsh LOS/NLOS environments. *IEEE Transactions on Signal Processing*, 61(9), 2243–2255.

Zhang, D., Liu, Y., Guo, X., Gao, M. and Ni, L. M. (2012). On Distinguishing the Multiple Radio Paths in RSS-Based Ranging. *IEEE INFOCOM*. IEEE, Orlando, USA.

Zhang, J., Salmi, J. and Lohan, E. S. (2013). Analysis of kurtosis-based LOS/NLOS identification using indoor MIMO channel measurement. *IEEE Transactions on Vehicular Technology*, 62(6), 2871–2874.

Zhang, S., Gao, S., Wang, G. and Li, Y. (2015). Robust NLOS error mitigation method for TOA-based localization via second-order cone relaxation. *Communications Letters IEEE*, 19(12), 2210–2213.

Zhuang, Y., Lan, H., Li, Y. and Elsheimy, N. (2015). PDR/INS/Wifi integration based on handheld devices for indoor pedestrian navigation. *Micromachines*, 6(6), 793–812.